

Study on bending properties and damage mechanism of carbon fiber reinforced aluminum laminates

Jiang Sun¹ , Xuejun Zhou² , Xiufeng Wei³, Yuesen Liu² , Jiawen Zhang² 

¹Tianjin University Renai College. 300000, Tuanbo New City, Jinghai District, Tianjin, China.

²Tianjin Sino-German University of Applied Science, School of Mechanical Engineering. 300000, Yashen Road, Jinnan District, Tianjin, China.

³Tianjin Tianfa General Factory Electromechanical Equipment Co. Xiaodian Branch, 300000, Beichen District, Tianjin China.

e-mail: sam_renai@163.com, zhouxuejun1978@163.com, 12690122@qq.com, 18669889350@163.com, zhangjiawenjx@163.com

ABSTRACT

Carbon fiber reinforced aluminum laminates (CARALL) are often subjected to bending loads in actual working conditions, resulting in some imperceptible intra-layer or inter-layer damages, such as matrix cracking, fiber fracture and inter-layer delamination, which degrade the mechanical properties of the structure. In this paper, the bending performance and damage mechanism of CARALL are tested and simulated by finite element simulation. Firstly, the mechanical properties are analyzed by three-point bending test, and the fracture morphology of the specimen after failure is photographed by scanning electron microscope, and the failure damage state from the microscopic perspective is analyzed. Secondly, the VUMAT subroutine with built-in three-dimensional Hashin criterion is introduced into abaqus. By comparing the finite element simulation and experimental results, the rationality and accuracy of using VUMAT subroutine to predict the failure behavior of Al-CFRP-Al laminates are verified. The results show that during the bending failure process, the aluminum alloy layer suffered local damage, and the carbon fiber layer suffered a large area of damage. The layer near the indenter was subjected to large stress concentration during bending, resulting in intensified interlayer interaction and serious damage. The crack began to expand downward along the stress and gradually became smaller as it expanded. The research results provide basic data reference for the bending performance and damage mechanism of fiber metal laminates (FMLs), and have important engineering application value for the optimization design of related structures.

Keywords: CARALL (Carbon fiber reinforced aluminum laminates); bending performance; damage mechanism; three-point bending test; finite element simulation.

1. INTRODUCTION

FMLs are laminated metal materials and composite materials in a multi-layer stacking manner through a certain processing technology. Figure 1 is a typical FMLs structure [1]. FMLs combine the advantages of composite materials and metal materials, and show excellent performance in fatigue resistance, impact resistance, specific strength, specific modulus, lightweight and applicability [2–6].

Carbon Fiber Reinforced Aluminum Laminates (CARALL), which is made of CFRP and aluminum alloy sheets, is considered to be the third generation of FMLs [7–9]. With its excellent comprehensive performance, it can shine in aerospace, military manufacturing, automobile production and other fields. Because of its large elastic modulus, carbon fiber can more effectively enhance the mechanical properties of materials such as tensile, bending and compression resistance when laminated with aluminum alloy [10–13]. And because the density of carbon fiber composites is significantly less than that of aluminum alloy materials, so that the laminate can effectively achieve the purpose of lightweight [14]. However, in the actual manufacturing, use and maintenance process, it is often subjected to bending load, resulting in some imperceptible intra-layer or inter-layer damage, such as matrix cracking, fiber fracture and inter-layer delamination, which seriously degrades the mechanical properties of the structure and seriously reduces the structural strength and service life. The bending performance of laminates is one of the important indexes to test the external force damage resistance of vehicle body structure, and its bending strength is also the key parameter of vehicle body structure design. Therefore,

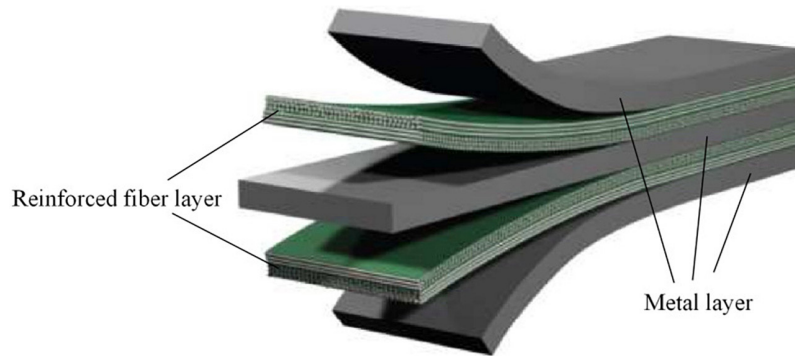


Figure 1: Structure diagram of fiber metal laminates.

the research on the failure mode prediction and damage process of CARALL under bending load is of great significance to improve the external damage resistance of CARALL structure and the design of carbon fiber composite body structure.

Domestic and foreign scholars have carried out a lot of research work on the bending performance and failure mechanism of CARALL laminates from the aspects of experimental analysis and numerical simulation, and have achieved rich results. DANIEL *et al.* [15] used the finite element simulation technology and the two-dimensional Chang-Chang damage criterion as the criterion to simulate the failure behavior of CARALL under bending load according to the tiebreak algorithm, and explored its damage mechanism. LIN *et al.* [16] used the VUMAT subroutine to establish the progressive damage model of CARALL three-point bending under the Abaqus/Explicit solver. The damage criterion of the fiber adopts the maximum strain criterion, and the damage failure criterion of the matrix adopts the Puck criterion, which effectively reveals the failure behavior and damage mechanism of CARALL three-point bending process. KUMAR *et al.* [17] showed by finite element (FE) simulation that in CARALL laminates, the failure is caused by delamination between layers near the middle of the laminates; HAICHAO *et al.* [18] used 2D Hashin and 3D Hashin VUMAT models to analyze and compare the finite element modeling of CARALL composite layer. They found that 2D Hashin and 3D Hashin models have similarities in predicting bending performance, mechanical response before peak load point and final failure mode, and emphasized that 3D Hashin model can accurately reveal the failure mechanism and failure propagation mechanism of CARALL. However, there are few studies on the bending performance and damage mechanism of CARALL, especially the failure mechanism of CARALL from the microscopic point of view.

In order to further understand the mechanical properties and damage mechanism of CARALL and predict its mechanical properties failure behavior, the failure mechanism of CARALL is revealed from the microscopic point of view by means of theoretical and numerical simulation [19]. Using scanning electron microscope to photograph the fracture morphology of the specimen after failure can effectively understand the failure damage state of the laminate from a microscopic perspective [20]. In order to more accurately restore the damage state of raw materials, the finite element simulation of the bending process of CARALL was carried out by using the VUMAT subroutine in Abaqus software combined with the three-dimensional Hashin criterion. Due to the relatively few studies on the mechanical properties of the new composite material CARALL, and its stress damage and failure are complex, the failure behavior prediction and morphology characterization are more difficult than traditional materials. Therefore, it is necessary to explore the bending performance and damage mechanism of CARALL.

2. PREPARATION OF AL-CFRP-AL LAMINATES

2.1. Aluminum alloy surface treatment

Al-CFRP-Al laminates are composed of 6061 aluminum alloy and T700 unidirectional carbon fiber prepreg. The chemical composition of 6061 aluminum alloy is shown in Table 1, and the thickness is 0.5 mm.

If the aluminum alloy is directly bonded to the prepreg, the interlayer cracking often occurs in the later stage, resulting in material damage. In order to enhance the interfacial bonding properties of the laminates, the surface of the aluminum alloy was anodized. Figure 2 is the surface treatment process of the aluminum alloy: first, the surface was polished with 180 # SiC sandpaper, and then subjected to acid-base corrosion treatment. After cleaning and drying, the anodic oxidation treatment was performed. The ultrasonic vibration cleaning was used to remove impurities. After alkali washing, deionized water was used to quickly rinse to avoid scratch defects on the surface of the sample.

Table 1: Chemical composition of 6061 aluminum alloy.

ELEMENT	MASS FRACTION (%)
Al	matrix
Mg	1.2
Fe	0.7
Si	0.6
Zn	0.25
Cr	0.2
Mn	0.15
Ti	0.15
Cu	0.15

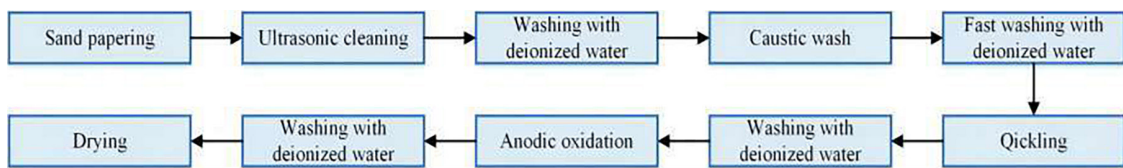


Figure 2: Aluminum alloy surface treatment process diagram.

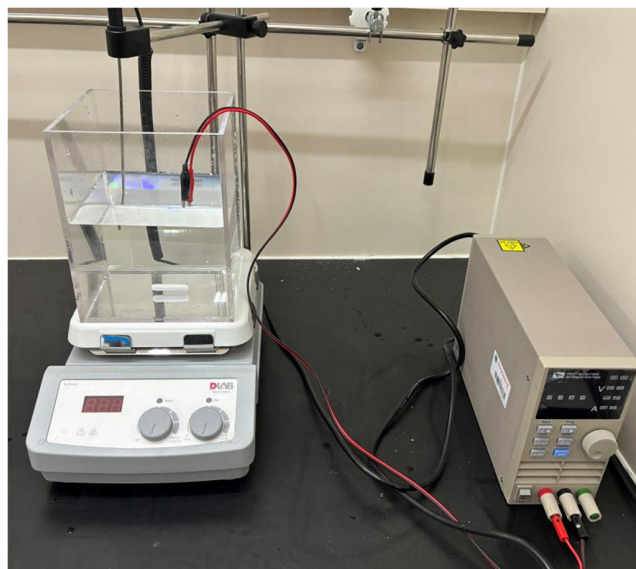


Figure 3: Anodizing equipment.

The anodizing equipment is shown in Figure 3. The system supplies a stable voltage through a DC power supply; the cathode is stainless steel plate, and the anode is aluminum alloy plate after acid and alkali corrosion treatment. The oxidation solution used is phosphoric acid solution; the thermometer is used to monitor and adjust the real-time oxidation temperature; the stirrer can make the ions in the oxidation liquid evenly distributed and improve the oxidation efficiency.

Table 2 shows the chemical composition and related process parameters of the phosphoric acid oxidation solution used in the system. After the surface of the aluminum alloy plate was anodized, it was dried with cold air for later use.

Figure 4 is the microstructure morphology of the aluminum alloy surface after anodizing. It is observed that a dense nano-scale oxide film is formed on the surface of the aluminum alloy after anodizing with phosphoric acid. The oxide film is a pore-like structure, which is neatly arranged on the surface of the aluminum alloy. This structure will help the resin to immerse, thereby improving the interface bonding strength of the aluminum alloy layer and the CFRP layer.

Table 2: Composition of oxidation tank liquid and process parameters.

DESIGNATION	PARAMETER
phosphoric acid	100 g/L
mains voltage	15 V~25 V
mixing speed	200 r/min
temperature	About 25°C
Time	10~20 min

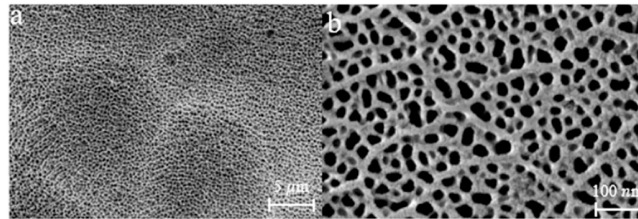


Figure 4: Micro-photographs of aluminum alloy surface: (a) low magnification; (b) High multiples.

Table 3: T700 carbon fiber prepreg material parameters.

FIBER SURFACE DENSITY (g/m ²)	RESIN CONTENT (%)	PREPREG DENSITY (g/m ²)	THICKNESS (mm)
125	42	215	0.125



Figure 5: Molding equipment.

2.2. Molding

The T700 carbon fiber prepreg was used, and the material parameters were as shown in Table 3. The laying direction was alternated by $[0^{\circ}/90^{\circ}]_{4s}$ to ensure the uniformity of the fiber arrangement inside the laminate. The epoxy resin is filled at the interface between the aluminum alloy and the carbon fiber layer to further strengthen the interlayer bonding performance of the laminate.

The molding process has high precision and good quality stability. Therefore, Al-CFRP-Al laminates were prepared by this process. The molding equipment is shown in Figure 5. The mold was brushed with release



Figure 6: Bending specimen.

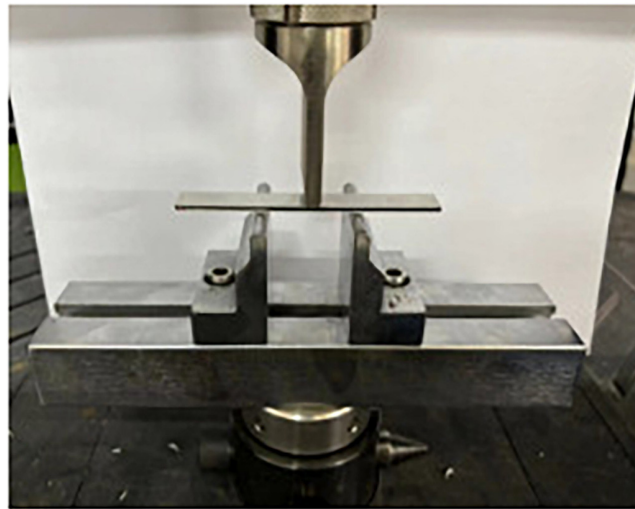


Figure 7: Bending test process.

agent before molding. In order to prevent the resin overflow of the prepreg during the molding process, the mold was set as a back-shaped frame. The mold was preheated first, and then the prepared material was placed in the mold. Then the mold was closed, and the closed mold was placed on the press table. Then the temperature was raised and raised. When the temperature of the upper and lower molds was raised to 370–380°C, the pressure was increased to 1.5–2.0 MPa and maintained for 120 min. After that, the pressure was unloaded and cooled at a rate of 2°C/min. When the temperature was reduced to 60°C, the mold was opened.

Waterjet cutting is a non-thermal effect cutting technology. Water flow and abrasives cut the workpiece in a high-speed impact manner, without thermal deformation, oxidation or cracks, which can ensure the integrity of the workpiece structure. Therefore, after molding, the water knife cutting method is used to cut into a bending sample of 100 × 13 × 2 mm, as shown in Figure 6.

3. EXPERIMENTAL PROCESS

3.1. Three-point bending test

The MTS universal testing machine was used to carry out the experiment. The radius of the specimen support and the indenter was 3mm, as shown in Figure 7. The loading rate is 2 mm/min, and the span ratio is 16:1, that is, 32 mm, which can ensure that the sample will not fall after bending under load. Composite materials often have multiple fracture points due to their multiple components. The maximum load before the first fracture of general materials is the maximum bending load. In the three-point bending experiment, the load is usually reduced to 90% of the maximum load as a failure criterion. This experiment uses the standard and conducts three sets of parallel experiments.

With the increase of load, the specimen will produce bending deformation at the stress point, and the degree of deformation will increase with the increase of load until the end of the experiment, as shown in Figure 8.

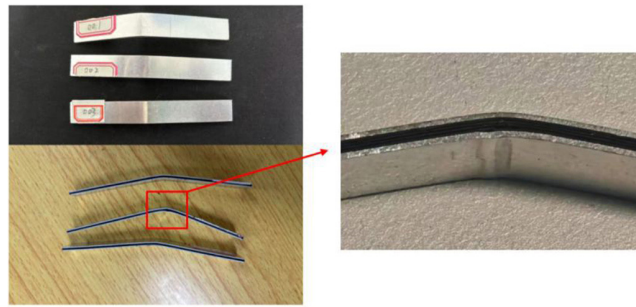


Figure 8: Damaged bending specimen.

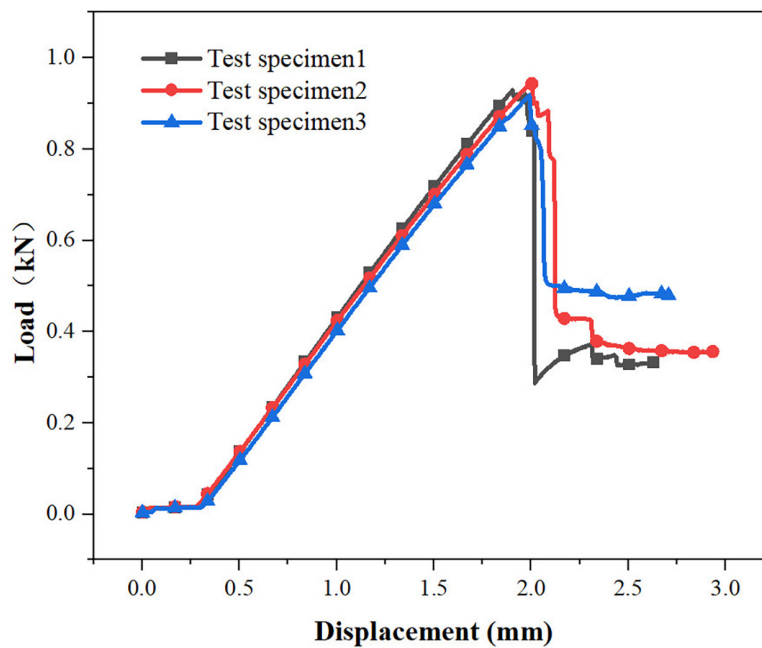


Figure 9: Load-displacement curve of Al-CFRP-Al laminates in three-point bending.

The whole sample did not break after the bending experiment, showing a plastic deformation state. There is no obvious fracture failure in the aluminum alloy layer, and finally plastic deformation occurs. The CFRP layer in the middle shows cracks, accompanied by a certain degree of interlayer dislocation. This phenomenon is mainly attributed to the inhomogeneity of stress distribution between different layers and the difference of interface strength. Based on the above observation and analysis, it can be inferred that the failure of the material bending process is mainly caused by the fracture of the fiber layer.

Figure 9 shows the three-point bending load-displacement curve of Al-CFRP-Al laminates. It can be seen that the ultimate bending load of the three experimental samples is above 900N, and the average bending strength is about 855 MPa by calculation. Before the first fracture, the bending stress and strain increase linearly, indicating that the material has elastic strain before this, and then the load drops directly. There is no obvious plastic deformation stage, and the load after the drop is much lower than 90% of the maximum load. Through the load-displacement curve, it can be judged that the reinforced fiber layer plays a dominant role in the bending process of Al-CFRP-Al laminates, which is mainly due to the high stiffness performance of carbon fiber composites. Due to the good ductility with the aluminum alloy layer, even if the fiber layer is broken, the whole sample is not completely broken, and the macroscopic whole only appears bending deformation, which avoids the instantaneous fracture of the carbon fiber material beyond the stress limit in the practical engineering application.

3.2. Fracture morphology analysis

After the experiment, the damage of the fiber layer on the fracture surface of the sample was observed under the scanning electron microscope. It was found that the aluminum alloy layer did not break. In order to avoid

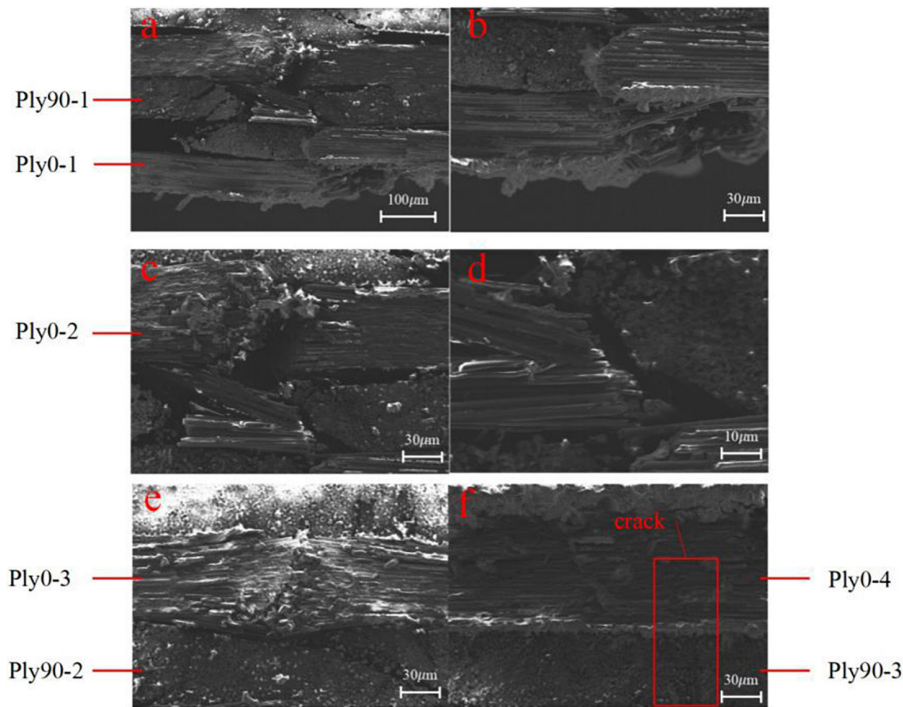


Figure 10: Microscopic morphology of fracture surface of three-point bending CFRP laminate.

resin volatilization during electron microscope scanning, the aluminum alloy and CFRP layer were separated by hot baking treatment. The microstructure of the carbon fiber composite layer was mainly studied. Figure 10 below is the micro-morphology of the fracture CFRP layer after the three-point bending test of the Al-CFRP-Al laminated plate. The carbon fiber layer is broken as a whole, and the closer to the indenter, the more serious the damage of the fiber layer. In the observation diagram (a) and (b), it was found that not only all the fiber bundles of Ply0-1 layer were broken, but also the fiber layers were misaligned and the bonding interface was separated. The matrix of Ply90-1 was broken, and some bases were even completely separated. It can be seen from Figures 10(c) and (d) that all the fiber bundles of Ply0-2 layer fractured along the tensile direction, and a small part of the fibers migrated from the matrix to the fracture of Ply90-1 layer due to extrusion. The figure 10(e) shows that the matrix of the Ply90-2 layer is completely broken under the bending load force, the crack extends to the bonding interface with Ply0-3, the Ply0-3 layer carbon fiber bundle is completely broken, and the overall structure does not appear dislocation and spalling. From figure 10(f), it is observed that the matrix of Ply90-3 layer is broken, and the crack extends to the middle of Ply0-4 layer. The carbon fiber bundle of Ply0-4 layer is partially broken near the indenter direction, and no obvious failure behavior is observed near the base part and Ply90-4 layer. The main reason for the above damage is that the CFRP layer is deformed as a whole under bending load. However, due to the small deformation space and large local stress in the '1' and '2' layers near the indenter direction, not only deformation tensile failure will occur, but also inter-layer extrusion will occur, resulting in large-area material damage and failure. The '3' and '4' fiber layers are far away from the stress loading point, and the load can be effectively transmitted to the surrounding area. The inter-layer interaction force is small, so the degree of damage is small.

4. FINITE ELEMENT ANALYSIS

4.1. Finite element damage model

The base and the indenter are set as a cylindrical discrete rigid body with a bottom radius of 3 mm, and the distance between the two bases is set to 32 mm according to the three-point bending experiment. Figure 11 is the geometric model of three-point bending.

According to the experimental conditions, the contact and constraint conditions are set in Abaqus software. As shown in Figure 12, the three rigid bodies of the support and the indenter and the sample are set to face-to-face contact. The main surface is the upper and lower surfaces of the sample, and the slave surface is the outer surface of the rigid body. The tangential contact type is set to 'penalty contact' considering friction factors, and the radial contact is set to frictionless hard contact. Referring to the experimental data, a 3.5 mm

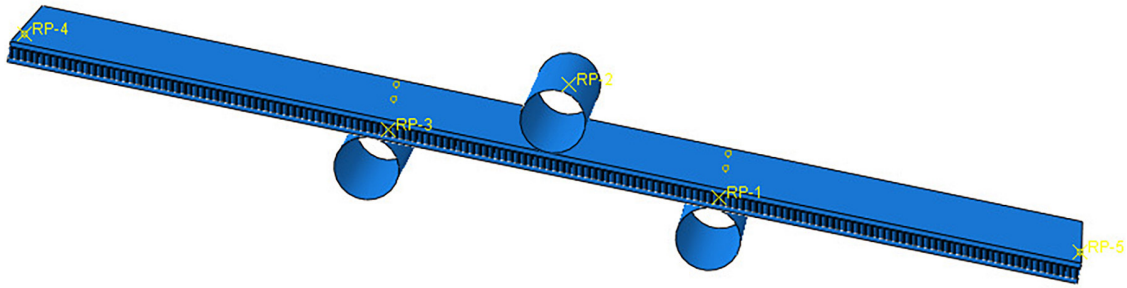


Figure 11: Three-Point bending geometric model.

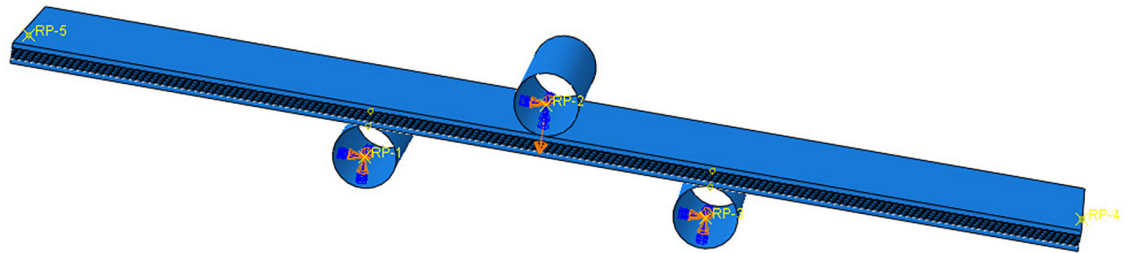


Figure 12: Three-point bending model constraints and load conditions.

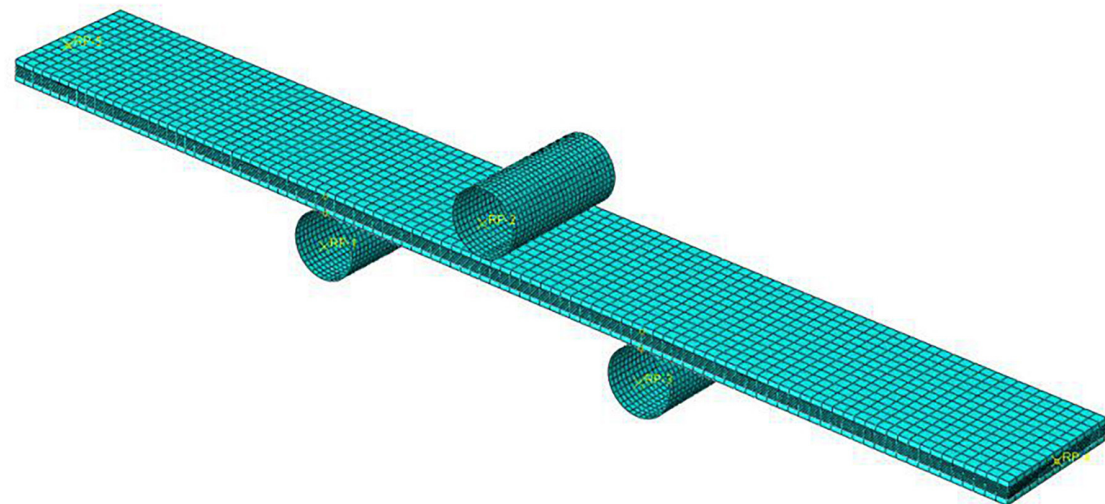


Figure 13: Triangular mesh division model with curved edges.

displacement load perpendicular to the surface of the laminated plate is set for the indenter, and the amplitude curve of the smooth loading is set. The degree of freedom in the other directions is 0, and the two bearing rigid bodies are completely fixed.

Then, the explicit dynamic analysis step is created in the analysis step module, and the historical variable output variable is set at the contact point between the indenter and the upper surface of the sample to output the load and displacement of the point. Because the whole sample will produce bending deformation during the bending process, the homogenization mesh is used. The discrete rigid body does not participate in the deformation, and the high-density mesh with a size of 0.5×0.5 mm is divided, as shown in Figure 13 below.

4.2. Failure criteria

Abaqus's built-in two-dimensional Hashin criterion can only be limited to the analysis of composite materials in two-dimensional stress state and damage state, and can not predict the damage situation in three-dimensional stress state. In the actual test, the damage situation of composite materials is generally relatively complex.

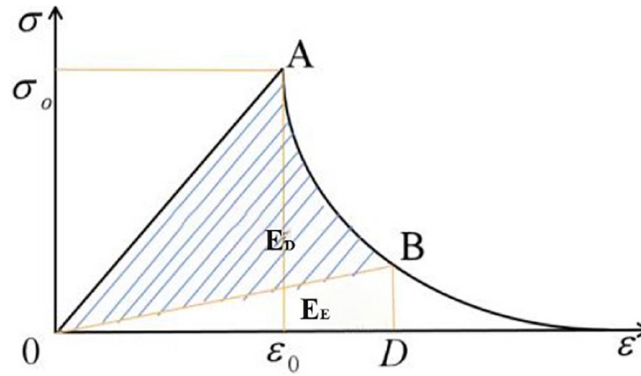


Figure14: Schematic diagram of energy dissipation in composite materials.

Therefore, the simulation of the failure behavior of composite materials in three-dimensional stress state is closer to the actual damage situation. Therefore, the VUMAT subroutine written in Fortran language is used in this paper. The VUMAT composite damage subroutine contains the three-dimensional Hashin failure criterion, and takes into account the stiffness degradation after the material begins to damage [21]. The energy calculation formula is as follows:

$$E_D = E_I - E_E = S_{OABD} - S_{OBD} \quad (1)$$

In formula (1), E_I is the internal energy, and the value is the area of the quadrilateral OABD of the curved surface in figure 14; E_E is the elastic energy, and the value is the area of the triangle OBD; and E_D is the dissipative energy, which is the area of the shaded part OAB in the figure.

Combined with the stiffness degradation of the composite material, the damage variable d is introduced as the criterion for judging the initial damage of the material. When $d = 0$, the material is not in the damage state; when $d = 1$, the material completely fails; when $0 < d < 1$, the material enters the damage state but not completely fails, and it also has a certain bearing capacity. The stiffness degradation matrix of the material is as follows:

$$M = \frac{\hat{\sigma}}{\sigma} = \begin{bmatrix} 1/(1-d_f) & 0 & 0 \\ 0 & 1/(1-d_m) & 0 \\ 0 & 0 & 1/(1-d_s) \end{bmatrix} \quad (2)$$

In formula (2), d_f , d_m and d_s represent fiber damage variable, body damage variable and shear damage variable respectively. When the VUMAT subroutine is used for calculation, the stiffness degradation matrix of the composite material is used as a function of the damage variable, and the bilinear evolution law is adopted. The matrix damage evolution law is the same as that of the fiber. For the four failure modes of fiber reinforced composites, the corresponding damage variable calculation formulas are as follows:

$$\left\{ \begin{array}{l} d_{fc} = \frac{\varepsilon_{f,1}^c}{\varepsilon_{f,1}^c - \varepsilon_{11}^c}, \quad \varepsilon_{f,1}^c = \frac{2G_{fc}}{X^T L_c} \\ d_{mc} = \frac{\varepsilon_{m,2}^c (\varepsilon_{22} - \varepsilon_{22}^c)}{\varepsilon_{22} (\varepsilon_{m,2}^c - \varepsilon_{22}^c)}, \quad \varepsilon_{m,2}^c = \frac{2G_{mc}}{Y^T L_c} \end{array} \right. \quad (3)$$

In Equation (3), ε^c is the critical failure strain under the compression failure mechanism, G is the fracture energy, L_c is the element characteristic strength, and its calculation method is shown in Formula (4).

$$L_c = \begin{cases} \sqrt{S} & \text{first-order tetrahedron} \\ \sqrt[3]{V} & \text{first-order hexahedron} \end{cases} \quad (4)$$

In the formula, S is the area of the quadrilateral and V is the volume of the hexahedron.

By introducing the VUMAT composite material damage subroutine in Abaqus, the parameters of carbon fiber composite materials can be set more accurately. At the same time, the subroutine has a three-dimensional Hashin criterion as the failure criterion, which can make the material damage more in line with the actual state and improve the reliability of the analysis results.

4.3. Damage mechanism

Figure 15 is the comparison of the stress-strain curves of simulation and experiment (sample 2). The overall trend of the two curves is roughly the same. Before reaching the maximum load, the stress increases linearly with the strain, but after reaching the limit load, it suddenly drops, and the material is damaged. Similar to the experimental scene, due to the incomplete failure of the material as a whole, secondary fracture will also occur in the future. This paper mainly studies the load loading and the failure state of the laminated plate during the primary fracture. The simulation results show that the maximum bending load is 970.6N, and the calculated bending strength is 896 MPa, which is slightly larger than the experimental data. Because the finite element simulation is usually based on an idealized mathematical model, the boundary conditions can be set more accurately, resulting in the simulation results may be better than the experimental results. However, the overall relative error is within 5%, and it is determined that the simulation results are effective.

Figure 16 below is the finite element simulation damage cloud diagram of the aluminum alloy layer of Al-CFRP-Al laminates. (a) is the upper plate, which is in direct contact with the indenter, and (b) is the lower plate. Through the analysis of the cloud map, it can be found that the upper and lower aluminum alloy layers are damaged below the indenter and spread along the surrounding area. The damage of the upper layer is slightly larger than that of the lower layer, and the damage variable is less than 1, indicating that the aluminum plate is not completely failed. In the actual experiment, the bending experiment of the aluminum alloy layer also did not appear obvious fracture, indicating that the simulation results were consistent with the actual results.

Figure 17 is the damage cloud diagram of CFRP layer after bending of the finite element model of Al-CFRP-Al laminated plate. (a) is the damage of 0° fiber layer. The cloud diagram results show that the four layers of 0° ply carbon fiber have fiber tensile failure, and the maximum damage variable is '1', indicating that

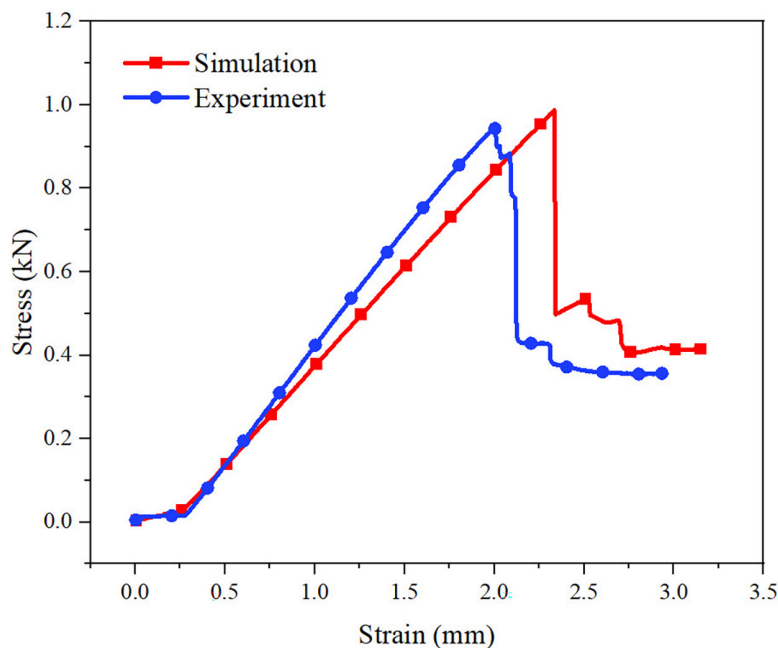


Figure 15: Stress-strain curve.

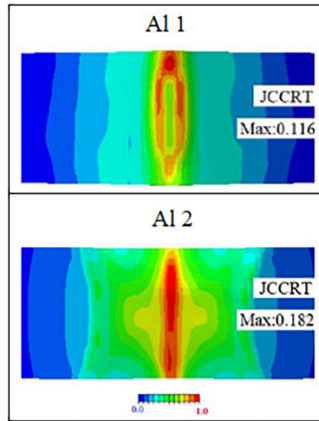


Figure 16: Aluminum alloy layer bending damage cloud map.

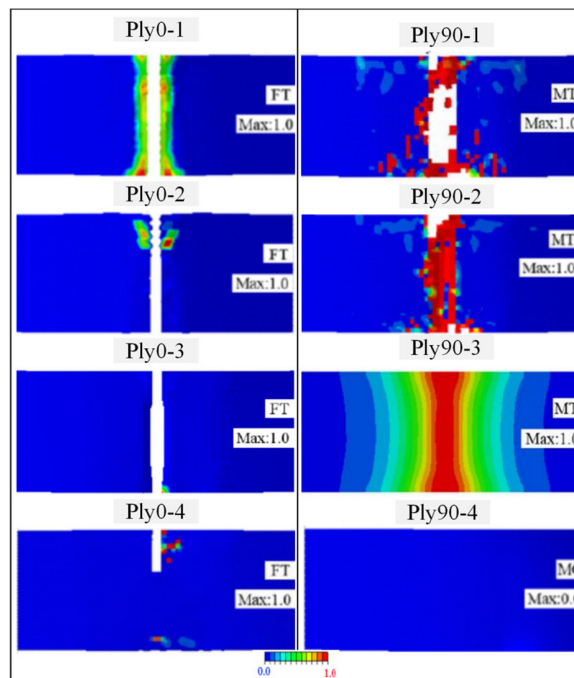


Figure 17: Damage cloud diagram of CFRP layer in three-point bending model.

it has completely failed. The failure position is directly below the indenter. Ply0-1, Ply0-2 and Ply0-3 layers are completely broken, and Ply0-1 is the most severely damaged. The damage extends from the fracture to the surrounding, and Ply0-4 layer is not completely broken. This is very consistent with the fracture morphology observed by scanning electron microscopy. (b) For the 90° fiber layer damage, the upper three layers of CFRP layers are judged to be the complete failure of the matrix tension. Ply90-1 and Ply90-2 are seriously damaged, so that the element mesh distortion is too large and deleted, and the model appears fracture. Although Ply90-3 does not break, it is also determined that the matrix at the stress point is completely invalid. The damage variable of Ply90-4, which is the farthest from the loading point, is '0', that is, no damage occurs. The damage cloud diagram of the CFRP layer is in good agreement with the fracture morphology observed above, which further verifies the accuracy of predicting the failure behavior of laminates through the VUMAT subroutine.

From the simulation results, the failure state of the bending damage model established by the VUMAT subroutine is in good agreement with the experimental situation. The ultimate bending load value predicted by the model is not much different from the actual value, which is within a reasonable range. The specific damage of each layer of the finite element model is also consistent with the observed actual situation. The microstructure of the CFRP layer is highly consistent with the damage state shown by the damage cloud map.

By analyzing the simulation damage results, we can intuitively understand the damage status and failure modes of each layer, and further understand the failure mechanism of Al-CFRP-Al laminates: aluminum alloy is not completely invalid in the bending process due to its good ductility. The CFRP layer and the interface layer are the main failure structures. Their large-area failure or even fracture during the bending process leads to the overall failure of the laminates. The upper structure bears the maximum stress during the bending process and is easily affected by stress concentration. The interlayer interaction intensifies, resulting in large-area failure. The lower structure is due to the transfer and diffusion of load between layers. The local bending stress is small and the damage degree is low.

5. CONCLUSIONS

In this paper, the three-point bending test of Al-CFRP-Al laminates was carried out, and the micro-morphology of the bending fracture of CFRP layer was observed. The fracture failure state of the fiber layer was analyzed. Then the three-point bending failure model of laminates was established, and the damage cloud diagram of each layer was analyzed to further explore the bending failure mechanism. The main conclusions are as follows: (i) Through the three-point bending experiment, the ultimate bending strength of Al-CFRP-Al laminates is measured to be about 855 MPa. The bending stress and strain in the load-displacement curve increase linearly, and the fracture failure occurs after the elastic deformation stage, and the load drops sharply. During the bending failure process of the laminated plate, the aluminum alloy layer did not break. The fracture crack of the fiber layer was observed by scanning electron microscope. It was found that the fracture crack of the fiber layer extended downward along the indenter. The upper carbon fiber was seriously damaged and the damage gradually decreased downward. (ii) Combined with the stress-strain curve of the bending process and the damage of the sample after the three-point bending test, it is judged that the main damage is the large area damage of the CFRP layer. The brittle fracture leads to the failure of the Al-CFRP-Al laminates. Because of its good ductility, most of the aluminum alloy is only plastic deformation, so the material is not completely broken, which protects the integrity of the material to a certain extent. (iii) Comparing the finite element simulation and experimental results, because the damage model is more idealized than the actual, the bending strength predicted by the simulation is slightly higher than the experimental results, but all within a reasonable range, the stress-strain curve trend is basically the same, and the fracture position and damage state are also consistent with the actual situation, which proves the rationality and accuracy of using the VUMAT subroutine to predict the failure behavior of Al-CFRP-Al laminates. (iv) In the process of bending failure, the finite element damage cloud diagram and fracture morphology of the sample are analyzed. It is concluded that the local damage of the aluminum alloy layer, the carbon fiber layer produces a large area of damage during the bending failure of the laminated plate, and the layer near the indenter is due to the stress concentration during the bending process. The interaction between the layers is serious, the degree of damage is large, and the crack propagates downward along the stress and gradually decreases. The failure mode of the 0° carbon fiber layer is fiber tensile failure, the 90° fiber layer is matrix tensile failure, and the Ply90-4 layer does not appear damage.

6. ACKNOWLEDGMENTS

The author thanks Tianjin Sino-German University of Applied Sciences, Tianjin Renai College and Tianjin Tianfa General Factory Electromechanical Equipment Co., Ltd. The authors appreciate all the anonymous referees for their valuable suggestions, which have helped us to improve the quality of the present manuscript.

7. BIBLIOGRAPHY

- [1] AZHDARI, S., FAKHREDDINI-NAJAFABADI, S., TAHERI-BEHROOZ, F., “An experimental and numerical investigation on low velocity impact response of GLAREs”, *Composite Structures*, v. 271, pp. 114123, 2021. doi: <http://doi.org/10.1016/j.compstruct.2021.114123>.
- [2] ELETRI, H., KORKMAZ, M.E., GUPTA, M.K., *et al.*, “A state-of-the-art review on mechanical characteristics of different fiber metal laminates for aerospace and structural applications”, *International Journal of Advanced Manufacturing Technology*, v. 123, n. 9, pp. 2965–2991, 2022. doi: <http://doi.org/10.1007/s00170-022-10277-1>.
- [3] FU, Y., CHEN, Y., YU, X., *et al.*, “Fiber metal laminated structural batteries with multifunctional solid polymer electrolytes”, *Composites Science and Technology*, v. 230, pp. 109731, 2022. doi: <http://doi.org/10.1016/j.compscitech.2022.109731>.
- [4] GAO, L., LI, Z., JIANG, S., *et al.*, “Dynamic impact behavior and notched fatigue life of GLARE laminates”, *Composite Structures*, v. 323, pp. 117449, 2023. doi: <http://doi.org/10.1016/j.compstruct.2023.117449>.

- [5] KAKATI, S., CHAKRABORTY, D., “Delamination in GLARE laminates subjected to oblique low velocity impact considering friction”, *European Journal of Mechanics. A, Solids*, v. 97, pp. 104817, 2023. doi: <http://doi.org/10.1016/j.euromechsol.2022.104817>.
- [6] XIE, J.M., ZHOU, X.J., SHE, C., *et al.*, “A review of FMLs performance test methods and index evaluation”, *Matéria (Rio de Janeiro)*, v. 28, n. 1, pp. e20230006, 2023. doi: <http://doi.org/10.1590/1517-7076-rmat-2023-0006>.
- [7] LI, A.B., XU, S.H., WANG, H., *et al.*, “Bond behaviour between CFRP plates and corroded steel plates”, *Composite Structures*, v. 220, pp. 221–235, 2019. doi: <http://doi.org/10.1016/j.compstruct.2019.03.068>.
- [8] BRITO JÚNIOR, C.A.R., PARDINI, L.C., ANCELOTTI JÚNIOR, A.C., “Obtenção das constantes elásticas efetivas sob condição dinâmica de um laminado híbrido para uso aeronáutico”, *Matéria (Rio de Janeiro)*, v. 25, n. 3, pp. e-12823, 2020. doi: <http://doi.org/10.1590/s1517-707620200003.1123>.
- [9] ASTA, E.P., CAMBIASSO, F.A., RÍOS, J.C., *et al.*, “Determinación de la tenacidad a la fractura J en laminados fibra-metal del tipo CARALL con láminas de aluminio 6061 y 1050”, *Matéria (Rio de Janeiro)*, v. 23, n. 2, pp. e12092, 2018. doi: <http://doi.org/10.1590/s1517-707620180002.0427>.
- [10] PAWLAK, A.M., GÓRNY, T., DOPIERALA, L., *et al.*, “The Use of CFRP for structural reinforcement-literature review”, *Metals*, v. 12, n. 9, pp. 1470, 2022. doi: <http://doi.org/10.3390/met12091470>.
- [11] PERVEZ, M.R., AHAMED, M.H., AHMED, M.A., *et al.*, “Autonomous grinding algorithms with future prospect towards SMART manufacturing: a comparative survey”, *Journal of Manufacturing Systems*, v. 62, pp. 164–185, 2022. doi: <http://doi.org/10.1016/j.jmsy.2021.11.009>.
- [12] KUANG, C., ZHOU, Y., ZHU, H., *et al.*, “Thermal and mechanical damage to carbon fibre reinforced composites with metallic fasteners under lightning strike”, *Thin-walled Structures*, v. 193, pp. 111280, 2023. doi: <http://doi.org/10.1016/j.tws.2023.111280>.
- [13] MARAS, S., YAMAN, M., “Investigation of dynamic properties of GLARE and CARALL hybrid composites: numerical and experimental results”, *Engineering Analysis with Boundary Elements*, v. 155, pp. 484–499, 2023. doi: <http://doi.org/10.1016/j.enganabound.2023.06.026>.
- [14] MIRZA, H.A., LANG, L., TABASUM, M.N., *et al.*, “An investigation into the forming of fiber metal laminates with different thickness metal skins using hydromechanical deep drawing”, *Applied Composite Materials*, v. 29, n. 3, pp. 1349–1365, 2022. doi: <http://doi.org/10.1007/s10443-022-10024-5>.
- [15] DANIEL, I.M., WERNER, B.T., FENNER, J.S., “Strain-rate-dependent failure criteria for composites”, *Composites Science and Technology*, v. 71, n. 3, pp. 357–364, 2011. doi: <http://doi.org/10.1016/j.compscitech.2010.11.028>.
- [16] LIN, Y., HUANG, Y.X., HUANG, T., *et al.*, “Characterization of progressive damage behaviour and failure mechanisms of carbon fibre reinforced aluminium laminates under three-point bending”, *Thin-walled Structures*, v. 135, pp. 494–506, 2019. doi: <http://doi.org/10.1016/j.tws.2018.12.002>.
- [17] KUMAR, R.G., ANIRBAN, M., ANIRBAN, B., “Damage analysis of carbon fiber reinforced aluminum laminate under short beam and single edge notch beam bend test”, *International Journal of Mechanical Sciences*, v. 198, pp. 106393, 2021. doi: <http://doi.org/10.1016/j.ijmecsci.2021.106393>.
- [18] HAICHAO, H., QIANG, W., BOYA, L., *et al.*, “Progressive damage behaviour analysis and comparison with 2D/3D hashin failure models on carbon fibre-reinforced aluminium laminates”, *Polymers*, v. 14, n. 14, pp. 2946, 2022. doi: <http://doi.org/10.3390/polym14142946>. PubMed PMID: 35890722.
- [19] SARAND, S.F., SHOKRIAN, M.D., SHELESH-NEZHAD, K., *et al.*, “The effect of electrophoretic deposition of carbon nanotubes onto carbon fiber on the interlaminar resistance of carbon reinforced aluminum laminates”, *International Journal of Adhesion and Adhesives*, v. 118, pp. 103192, 2022. doi: <http://doi.org/10.1016/j.ijadhadh.2022.103192>.
- [20] TALREJA, R., “Assessment of the fundamentals of failure theories for composite materials”, *Composites Science and Technology*, v. 105, pp. 190–201, 2014. doi: <http://doi.org/10.1016/j.compscitech.2014.10.014>.
- [21] SHE, C., XIE, J.M., MAO, Z.Y., *et al.*, “Molding preparation and tensile properties test of carbon fiber reinforced aluminum laminates”, *Matéria (Rio de Janeiro)*, v. 28, n. 4, pp. e20230250, 2023. doi: <http://doi.org/10.1590/1517-7076-rmat-2023-0250>.